Piloting Melt Synthesis and Manufacturing Processes to Produce C-$LiFePO_4$: Preface

Gregory S. Patience,[1]* Jamal Chaouki,[1] Mohammad Latifi,[1] Mickaël Dollé,[2] Patrice Chartrand,[1] Wojciech Kasprzak,[3] Xueliang Sun,[4] Tsun-Kong Sham,[5] Guoxian Liang[6] and Pierre Sauriol[1]

1. *Department of Chemical Engineering, Polytechnique Montréal, Montréal, QC, Canada*
2. *Department of Chemistry, University of Montréal, Montréal, QC, Canada*
3. *CanmetMATERIALS, Natural Resources Canada, Hamilton, ON, Canada*
4. *Mechanical and Materials Engineering Department, Western University, London, ON, Canada*
5. *Chemistry Department, Western University, London, ON, Canada*
6. *Johnson Matthey Battery Materials, Candiac, QC, Canada*

Since Goodenough's team laid the foundation to apply $LiFePO_4$ as an alternative to lithium cobalt oxide for Li-ion positive electrodes,[1,2] Web of Science (WoS)[3] has indexed over 6000 articles related to lithium iron phosphate—LFP. Manufacturers synthesize LFP with both solid state and solvent assisted hydrothermal technology. Both have their advantages and disadvantages but society requires inexpensive batteries for automobile applications and fixed electrical storage. Here we scale up each step of the nascent melt synthesis process, which has the potential to displace the current commercial technology because of its superior economics related to raw materials. The research challenges include raw material selection, melt synthesis conditions, thermodynamics, micronization to form nano-powders, followed by spray drying, and carbon coating.

Keywords: comminution, electrochemical performance, lithium iron phosphate, structural characterization, thermodynamics

INTRODUCTION

Both industry and academia continue to develop materials and applications related to lithium iron phosphate (LFP) for the positive electrodes (cathodes) of batteries. The pioneering article from Goodenough's group was cited 5000 times.[1] Web of Science[3] (WoS) indexed 6200 articles since 1997 and most were in journals that they assign to multidisciplinary materials science, electrochemistry, and physical chemistry (Table 1). Fewer than 250 articles are in journals that WoS assigns to chemical engineering, which ranks it 12th among the scientific categories. The weighted mean impact factor ($\bar{N}_{IF}$) of the journals that publish the top 100 cited articles is 4.8, which is considerably higher than the mean impact factor of WoS (2016) at 1.3. The top 3 journals—*Journal of Power Sources*, $N_{IF} = 6.3$, *Electrochimica Acta*, $N_{IF} = 4.8$, *Journal of the Electrochemical Society*, $N_{IF} = 3.0$—published 25 % of all the articles. Articles published before 2015 have been cited on average 40 times with a median of 15.

Derwent[4] classifies 4390 patents into multiple subject categories dominated by engineering, energy & fuels, and chemistry (Table 1). Energy & fuels and multidisciplinary chemistry—ranked 4th and 5th with respect to WoS category—are in common with the Derwent patent subject fields. A recent highly-cited patent claims a process to coat the surface of lithium iron battery cathodes/positive electrodes at a lower cost with improved high temperature sintering stability.[5] The highest cited patent for LFP cathodes reduces energy demand and simplifies the process through spray drying and micronization.[6] Miyagi et al.[7] invented a lithium secondary battery that has been cited most. Inventors and assignees file most of the patents in a limited number of countries: of the cited patents, 3572 are filed in China, 173 in Japan, 172 in USA, 97 in Germany, 93 in Korea, and 182 assigned to WO.

Bibliometric maps group related research into clusters and identify work streams within clusters and between clusters. The LFP bibliometric map groups research related to LFP characterization, transport properties, and chemistry (blue),[8–10] manufacturing technologies (red), LFP electrical performance, behaviour, storage, stability, and thermal properties (green),[11,12] and applications and cell performance (yellow).[13] Nanoparticles and nanocomposites are together with the manufacturing cluster. Synthesis techniques include hydrothermal,[14,15] solid state reaction,[16] coprecipitation,[17,18] solvothermal,[19–22] mechanochemical,[23] sol-gel,[24] and spray pyrolysis (ultrasonic).[25–30] Less common techniques include the melt synthesis and microwave (often combined with a hydrothermal treatment)[31–34] and radio frequency magnetron sputtering.[35]

MELT SYNTHESIS

In 2005, researchers at the Université de Montréal uncovered the remarkable thermodynamic stability of LFP in the molten state at temperatures even above 1000 °C. Solid state synthesis

* *Author to whom correspondence may be addressed.*
E-mail address: gregory-s.patience@polymtl.ca
Can. J. Chem. Eng. 97:2189–2195, 2019

DOI 10.1002/cjce.23479
Published online 19 June 2019 in Wiley Online Library (wileyonlinelibrary.com).

Table 1. Lithium iron phosphate categories. WoS[3] indexed 6200 articles with lithium iron phosphate in the search category *topic*. Most of the journals that published article belong to four categories. Derwent[4] indexed 4390 patents with "lithium iron phosphate" as the sole keyword under the *topics* search category. Many of the patents appear in multiple categories

Rank	WoS categories	N_j	Derwent Subjects	N_p
1	Multidisciplinary Mat'l Sci.	2552	Engineering	4584
2	Electrochemistry	2296	Energy & Fuels	4227
3	Physical Chemistry	2097	Chemistry	4174
4	Energy & Fuels	1335	Polymer Science	1507
5	Multidisciplinary Chemistry	716	Instrumentation	1094
6	Condensed Matter Physics	675	Transportation	622
7	Applied Physics	519	Computer Science	340
8	Nanoscience & Nanotechnol.	519	Communication	190
9	Coatings & Films Mat'l Sci.	373	–	149
10	Electrical & Electronic Eng.	327	Metallurgy & Metall. Eng.	135
11	Metallurgy & Metall. Eng.	301	Imaging Sci.	44
12	Chemical Engineering	247	Materials Science	31

reach 500–700 °C, which is well below the melting point of LFP. To achieve high quality battery materials requires relatively pure feedstocks and fine powders ($d_p < 10$ μm).[37,38] On the contrary, feedstock selection for melt synthesis processes are broader and coarser, which allowed the team to consider lower grade minerals at a much lower cost. A series of concept validation trials, generally limited to the lab-scale, ensued, leading to patents[39,40] and articles[41,42] describing the discovery and work. A few years later, we established a research team drawing expertise from engineers for scale-up of melt synthesis processes at Natural Resources Canada CanmetMaterials (NRCan), scientists from Western University (WU) for detailed microscopy analysis, specialists in thermodynamics, particle technology, and scale-up from Polytechnique Montréal, and an original member from Phostech Lithium and the Université de Montréal that developed the concept at the laboratory scale. The process scale-up and fundamental research was supported financially through the Automotive Partnership Canada and Johnson Matthey Battery Materials. It begins with heating reactants to melting temperature followed by casting/cooling under controlled conditions to form rectangular cuboid ingots with the ideal microstructure and subsequent composition (Figure 1).[37,38] A jaw crusher reduces the 200 mm blocks to mm size particles. A roller grinder and wet media mill produce nanometric size particles. A spray dryer removes the water forming 10 μm agglomerates, which are then pyrolyzed and the carbon forms a thin film on the primary nanoparticles.

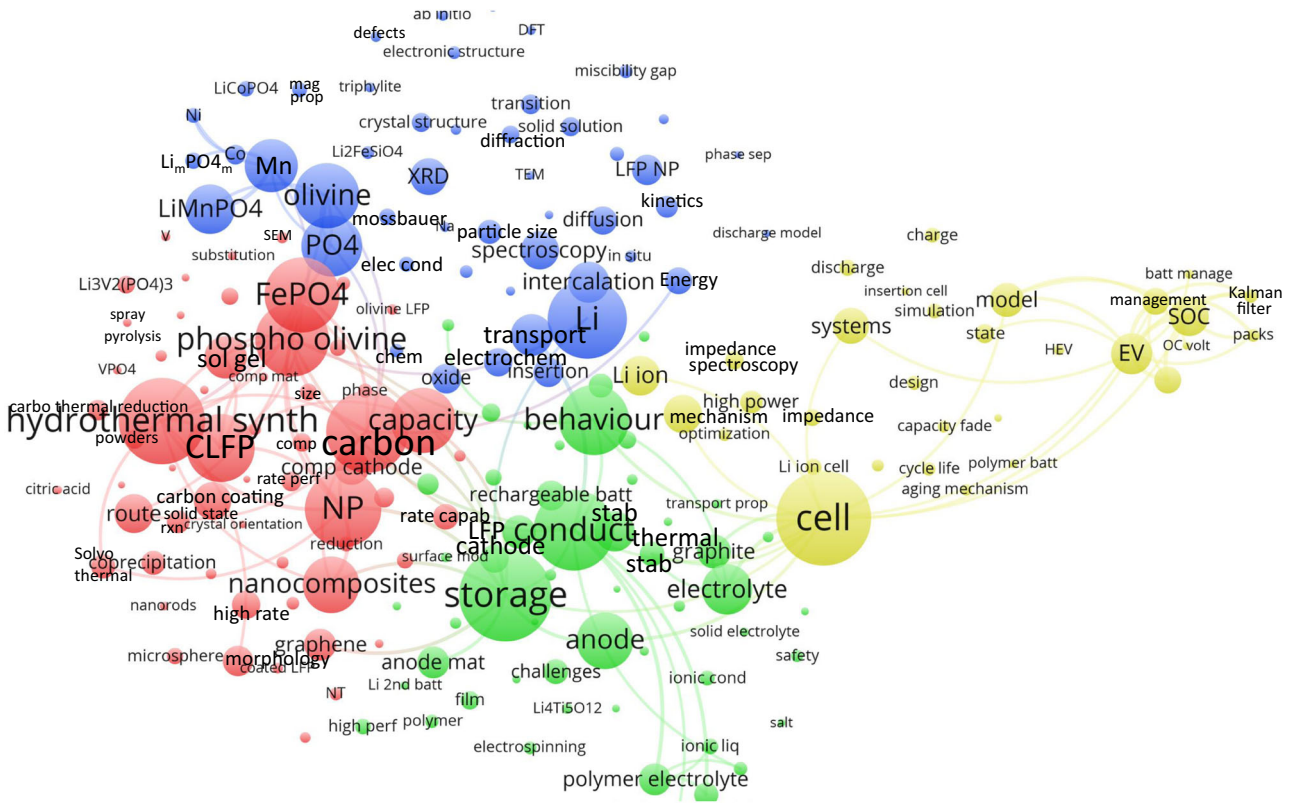

Figure 1. Lithium iron phosphate bibliographic map including 6200 articles that WoS indexed from 1997–2017.[3,36] The size of the symbols correlates with the number of occurrences of each keyword in an article. The largest circles in the plot are cell with 463 occurrences, storage (452), carbon (400), and conductivity (394). The smallest circles represent 37 occurrences. We excluded 13 keywords with over 500 occurrences, including: Li ion battery (3779), LFP (3091), electrochemical properties (1793), cathode materials (1720), cathode (1144), performance (1142), electrode (813), composites (717), battery (678), rechargeable Li ion battery (657), temperature (578), iron (557), and electrode material (532).

This special collection of articles summarizes preliminary results of the collaboration and includes thermodynamic modelling, reactants pre-treatment, melt synthesis operation, milling the LFP ingots to sub-micron particles, spray-drying LFP nanoparticle suspensions, carbon coating, electrochemical performance, and structural characterization of LFP.

Fe^3 REDUCTION DURING MELT SYNTHESIS OF $LiFePO_4$, SAURIOL ET AL.[43]

Induction furnaces operating up to 1250 °C produced 5 kg batches of LFP from coarse 509 μm Fe_2O_3. Fe^{3+} can be reduced by Fe, carbon, CO, and H_2 at high temperatures. Adding CO and H_2 accelerates the reaction rate. Fe metal extends the graphite crucible lifetime but is more effective when it is premixed with the feedstock, otherwise it agglomerates because of the eutectic in the $LiPO_3 - Fe - Fe_2O_3$ system. The reaction rate was proportional to the surface area of the base of the crucible for experiments in the absence of alternate reducing agents and kinetic data derived from the induction syntheses extrapolated well to lower temperature syntheses in laboratory scale resistive box furnaces. The stoichiometric mass fraction of Fe^{2+} in pure LFP is 35.4 % while considering the reactants purity and stoichiometric ratios, the theoretical maximum was 34.6 %. Here, with improvement to reduction reaction rate and atmosphere protection, we produced ingots with Fe^{2+} content ranging from 30.1–34.6 %. With respect to the bibliometric map (Figure 2), this study activity mostly lies in the red cluster describing the synthesis routes with some elements of characterization and kinetic belonging to the blue cluster.

CHEMICAL SPECIATION AND MAPPING OF THE Si IN Si DOPED LFP INGOT WITH SYNCHROTRON RADIATION TECHNIQUE, BANIS ET AL.[44]

Melt-synthesis from commodity grade reactants instead of high purity fine chemicals can contaminate the LFP. These contaminants could be present as substituted species in the LFP structure or as secondary or even tertiary phases. Low-cost iron-ore concentrate as a source of iron oxide[45,46] modified the lattice parameter and cell volume of the LFP. Despite a slightly lower capacity, the capacity retention is better. Si K-edge XANES spectra identify the chemical state of Si and its local electronic and atomic structure in LFP: in the absence of Mg, quartz type Si impurities form.

Close to 10 % of LFP articles in WoS mention doping to improve the charge/discharge properties, and other performance characteristics. Metals generally replace Fe and Li ions, while Si and F replace P and O, which increase electronics conductivity by up to 3 orders of magnitude.[47] Adding metals, like Zn, Pt, and Pd, enlarges the lattice volume,[48–50] while substituting bivalent cations like Ni, Co, and Mn, for Fe -sites improves rate performance and cycle stability.[51] The voltage potential in $LiMPO_4$ systems are 5.1 V for Ni, 4.8 V for Co, 4.1 V for Mn, and 3.5 V for Fe. However, the conductivity in Mn systems is lower compared to Fe. Adding vanadium increases the rate of charge/discharge capacity,[52] while Hu et al.[53] report the that Mg and Ti have no effect on electrochemical performance. Most of this study is equally divided between the red, green, and blue clusters—process, characterization, and electrical performance.

Figure 2. Lithium iron phosphate melt synthesis process steps.

VISUALIZATION OF THE SECONDARY PHASE IN LFP INGOTS WITH ADVANCED MAPPING TECHNIQUES, LIU ET AL.[54]

As many as 250 articles in WoS mention both LFP and impurities (or the lack of impurities). Like Banis et al.,[44] the keywords cited in these articles are divided evenly amongst the same clusters—red, green, and blue. While dopants are added to improve electrochemical properties, impurities can form secondary phases within the bulk of LFP crystals. Since the melt synthesis process allows us to work with less pure feedstocks, it becomes more important to identify the distribution of the impurities and detrimental secondary phases that form during the solidification process. XRD quantifies the concentrations of the phases but synchotron based Raman, energy dispersive spectroscopy (EDS), and micro x-ray fluorescence (XRF) mapping demonstrate how the impurities and secondary phases are distributed.

MODELLING OF PHASE EQUILIBRIA OF $LiFePO_4 - FePO_4$ OLIVINE JOIN FOR CATHODE MATERIAL, PHAN ET AL.[55]

A thermodynamic model for the olivine $LiFePO_4 - FePO_4$ has been proposed that gives the Gibbs energy of the solution as a function of composition and temperature by taking into account the long-range ordering of Li/Fe^{2+} and vacancy/Fe^{3+} substitution at the $Li_{0.6}FePO_4$ composition. A supercell of 5 chemical formulae has been defined, in agreement with the x-ray diffraction and selected area electron diffraction patterns of the $Li_{0.6}FePO_4$ sample annealed at 623 K of Furutsuki et al.,[56] which confirms the existence of a supercell microstructure corresponding to long-range-order. The model is calibrated with experimental and density functional theory data, and reproduces the 3 olivine-olivine miscibility gaps below 680 K. The isothermal the Gibbs energy curves, as a function of lithiation/delithiation are then converted to open circuit voltage, and interpretation of phenomenon associated to spinoidal decomposition during fast charging/discharging of the Li is given. The model will be further extended to take into account particle size effects down to tens of nanometers, and the coherency of the miscibility gap (where no lattice mismatch is observed between the 2 olivine phases during cycling). With respect to the bibliometric map, this study relates most to the blue and yellow clusters.

$Li_2O - P_2O_5$, LITHIUM BATTERY, DSC-TGA, MODIFIED QUASICHEMICAL MODEL, THERMODYNAMIC MODELLING, PHASE DIAGRAM, JIN ET AL.[57]

Jin et al.[57] applied the modified quasichemical model with sublattices I and II, $(Li^{1+})^{(I)}(O^{2-}, Va^{1-})^{(II)}$, to characterize the $Li_2O - P_2O_5$ liquid phase. The model accounts for first-nearest neighbours and second-nearest neighbours. They considered Li_2O and Li_2O_2 solid phases as stoichiometric compounds while the gas phase—with Li, Li_2, O, O_2, O_3, LiO, Li_2O and Li_2O_2—they assumed was ideal with the Gibbs energy per mole of species from the SGTE database.[58] The $Li_2O - P_2O$ phase diagram with optimized model parameters characterize the experimental transition temperatures reported in the literature well. The work reported in this study corresponds mostly with the blue cluster of the bibliometric map, and is supporting development work in the red cluster of the bibliometric map.

ULTRASOUND ASSISTED WET STIRRED MEDIA MILL OF HIGH CONCENTRATION $LiFePO_4$ AND CATALYSTS, LI ET AL.[59]

Molten LFP poured into 200 mm rectangular cuboid molds forms ingots that we mill to a submicron sized powder. The comminution steps include a jaw crusher that reduces the ingots to 1000 μm granules, a rolling mill that drops d_p to 50 μm, and finally a wet media mill that brings the size down to 0.2 μm. The energy input to reduce the particle size increases as the d_p becomes smaller; thus, the last step affects the economics of the micronization process most. Preliminary trials demonstrated reproducible particle size distribution in a laboratory scale Netzsch mill with up to a mass fraction of 30 % solids but with surfactant.[60] Here, we report an ultrasonic assisted wet media milling process that micronizes suspensions with as much as a mass fraction of 60 % solids.

Wet media mill performance and cost depend on the mass fraction of solids in the suspension, material characteristics, and surfactant concentration. Particles form clusters as they fragment (comminute). Consequently, grinding efficiency decreases exponentially with time. Maximum solids LFP concentrations are on the order of a mass fraction of 30 % solids. This study operated at a 2 fold higher mass fraction by introducing an ultrasonic horn in the faceplate of the milling chamber. Maximizing solids mass fraction increases throughput, but also reduces the energy demand for dewatering/drying. The cavitating bubbles generated by the ultrasound detached the nanoparticles from larger mother particles, thereby increasing the contact surface between the yttria stablilized media (YSZ) with the LFP. The grinding media (YSZ) was 0.3–0.4 mm in diameter and the mill operated at a surfactant-to-LFP mass ratio of 0.008. It took 105 min to reduce the particle size from 35–0.2 μm at a throughput of 0.68 $g^{-1} \cdot g^{-1} \cdot h^{-1}$ (LFP:media). The energy input from the ultrasonic horn was 350 $W \cdot h$.

Seldom do researchers cite milling as a keyword but 278 papers mention milling in the abstract, which places this operation among the top 20 processes of LFP manufacturing. Researchers either mix precursors and reduce agglomerates with ball milling and/or reduce the particle size after the synthesis step. Drezen et al.[61] produced $LiMnPO_4$ particles at 140–220 nm through sol-gel synthesis and reduced the powder to 90–130 nm in a Retsch PM 4000 high energy dry ball mill with a mass fraction of 20 % acetylene. Oh et al.[25] followed ultrasonic spray pyrolysis with dry ball milling. The optimal LFP particle size range to reach high energy density varies from 150–200 nm. Particle diameters lower than this have higher carbon content that reduces the LFP concentration and packing densities may also suffer.

INFLUENCE OF ATOMIZATION CONDITIONS ON SPRAY DRYING LITHIUM IRON PHOSPHATE NANOPARTICLE SUSPENSIONS, RIGAMONTI ET AL.[62]

Wet media milling produces a stable nano-particle suspension but requires an additional step to remove the dispersant (water) to make a dry powder. Spray drying is a high throughput, large scale unit operation that desiccates powders economically. Since 1994, as many as 50 articles indexed by WoS mention spray drying in combination with sol-gel synthesis,[63] carbothermal reduction,[64] solid state reaction,[65] and co-precipitation.[66] Several studies introduce multiple carbon sources—starch,[67] glucose and oxalic acid,[68] carbon nanotubes,[69] and PVA[70]—then calcine the solids at temperatures as high as 800 °C. Because of its strong technology component, spray drying belongs to the red cluster of subjects with the other manufacturing processes.

When LFP nanoparticle suspensions dry in furnaces, they are susceptible to oxidation, sintering, and Li_3PO_4 may segregate and come to the surface. Further, the primary particles agglomerate into large secondary particles resulting in a non uniform particle size distribution. Spray drying residence times in commercial facilities are on the order of tens of seconds thus material properties are better preserved versus rotary kilns with much longer residence times. A Yamato GA-32 (120 mm (ID) spray dryer, operating at an atomization gas velocity from 140–350 $m \cdot s^{-1}$ produced semi-spherical doughnut-shaped secondary particles that ranged from 3–10 μm[71]; at gas velocities from 50–140 $m \cdot s^{-1}$, larger spherical particles formed that varied from 10–20 μm. Increasing chamber temperature increased surface area and mesoporosity. A two-parameter skew normal distribution accounts for > 98 % of the variance in the particle size distribution data.

GAS-PHASE CARBON COATING OF $LiFePO_4$ NANOPARTICLES, AGHAEE-SARBARZE ET AL.[72]

Low electric conductivity and ionic conductivity are drawbacks of LFP while its advantages as a cathode material include, low cost, long cycle life, high energy density, and highly safe operation in a battery cell. To achieve acceptable ionic conductivity, LFP powders are micronized to the nanometric size. Coating LFP nanoparticles with a layer of conductive carbon like graphite improves their electrical conductivity, and limits particle growth on cycling, which is a cause of premature failure of Li ion batteries. However, conventional solid or liquid carbon coating processes have some limitations such as excess deposited carbon (dead-weight), heterogeneous layer, and undesired carbon type. Furthermore, inexpensive liquid- and solid-based carbon sources introduce impurities detrimental to battery performance when they are derived from waste streams of other industries. A fluidized bed chemical vapour deposition (FB-CVD) process introduces a gaseous carbon precursor—propylene, glycerol, acetylene, for example—that better controls the carbon coating thickness, uniformity, and carbon type: (1) the gas-phase carbon precursor easily diffuses in the matrix to reach LFP nanoparticles directly; (2) trace contaminants such as sulphur, alkali and alkali-earth metals, phosphorus, and oxygen are lower; and (3) energy intensive upstream vaporization steps are unnecessary. The FB-CVD operating at 700 °C with propylene as the precursor and Geldart group B secondary particles,[73] produced a powder with a uniform carbon layer at less than 10 nm thick that neither sintered nor agglomerated.

With respect to the bibliometric map, this study relates most to the red cluster with nanoparticles and synthesis methods. Over 30 articles in WoS mention chemical vapour deposition in the abstract, which ranks it among the top 200 LFP subjects. Only two articles mention fluidized bed reactors in relation to LFP—emulsion drip combustion in a fluidized bed[74] and ethylene catalytic chemical CVD.[75]

KINETICS OF THE DEHYDRATION OF LITHIUM DIHYDROGENPHOSPHATE, YARI ET AL.[76]

Production of lithium iron phosphate (LFP) via melt-synthesis method is possible with a wide range of starting materials. Precursors (like LiH_2PO_4, $NH_4H_2PO_4$, Li_2CO_3, FeC_2O_4) release large volumes of various gases while heating or during reaction in the molten state. Lithium metaphosphate ($LiPO_3$) is an ideal

material for melt synthesis[45,46] that reacts with iron oxide (Fe_2O_3) under reducing conditions, to high purity LFP in the molten state. However, $LiPO_3$ (LPO) is not commercially available. It can be produced by degassing of the commercially available lithium dihydrogenphosphate (LiH_2PO_4) at temperatures as low as 400 °C.

This article investigates the thermal decomposition of LiH_2PO_4 (LHP) to the final product of LPO. The decomposition progresses in a stepwise manner forming intermediates $Li_2H_2P_2O_7$ (L2), $Li_5H_4P_5O_{17}$ (L2.5), $Li_3H_2P_3O_{10}$ (L3), and $Li_4H_2P_4O_{13}$ (L4) before forming $LiPO_3$. TGA profiles of the reaction from ambient temperature to 400 °C for heating rates ranging from 1–30 $°C \cdot min^{-1}$ were obtained and the results analyzed using model-free isoconversional analyses. The results of the analyses provided activation energy estimates at various conversion extents following the Vyazovkin integral method.[77] The TGA profiles were then fitted using a kinetic model. The model was refined as needed by adding reaction steps as needed. The results of the modelling effort is a 5-step reaction scheme corresponding to the successive decomposition of LiH_2PO_4 LHP → L2 → L2.5 → L3 → L4 → LPO with 7 reactions. The first step, corresponding to the LHP → L2 decomposition, was modelled using 3 series/parallel reactions for solid surface reaction, viscous/liquid surface reaction, and core reaction. The complexity of the model is mostly due to melting and decomposition overlap. The test conditions with heating rates < 3 °C tend to deviate more from the others due to sintering or particle growth.

A benefit of such low temperature decomposition of the LHP to LPO is that the product is solid and can be stored, transferred, and mixed along with the other solid reactants during melt synthesis. Previous production[45,46] from molten LPO required casting, melting, and crushing and/or grinding before synthesis. Similar decompositions can be achieved with separate sources of Li and P leading to solid phase LPO, while mitigating the gas evolution.

The research described in this paper belongs to the red (synthesis) and blue (characterization) clusters.

MELT-SYNTHESIS OF $LiFePO_4$ OVER A METALLIC BATH, VILLAZON ET AL.[78]

A wider range of low cost raw materials are possible with the melt synthesis process compared to solid-state or hydrothermal processes. However, remaining unconverted secondary phases and impurities prejudice the electrochemical properties of LFP. Secondary phases segregate outside the LFP structure for non-stoichiometric precursor mixtures. For example low cost iron precursors—Si, Ca, Mg, Mn, Al—modify the unit cell parameters while creating defects in the olivine structure, which might require additional expensive purification steps. Rather than inductively heating the melt in a graphite crucible, this contribution adopts and modifies the Pilkington process developed to produce thinner, polished flat glass surfaces. Here, a tin or silver bath heats the LFP reactant powders. The metallic bath heats the powders and shields it from the container walls. Furthermore, the bath extracts impurities that have an affinity to the metal. The LFP electrical capacity with a tin bath reached 156 $mA \cdot h \cdot g^{-1}$, while it achieved 161 $mA \cdot h \cdot g^{-1}$ with a silver bath. Li, Fe, and P accumulating in the silver phase did not impact the quality of the product LFP. The lower discharge capacity in the sample from the tin bath was due to tin migrating into the LFP phase and forming secondary, segregated phases. The mass fraction of the bath of metal (tin or silver) in the LFP ingot varied from 1–4 % for tin and was 160 ppm for silver. The iron content of the metal layer after synthesis ranged from 2.4–13.6 % for the tin bath and 0.6 % for the silver bath.

Challenges remaining to develop a viable commercial process include: viscosity, mass transfer during heating, solidification, reaction kinetics, and the thermodynamics of the multi-component system Fe-P-O-Ag-C. The paper touches the red cluster concerning processing, the blue cluster related to thermodynamics and characterization, and the yellow cluster that deals with electrochemical properties.

FLAME-ASSISTED SPRAY PYROLYSIS OF LITHIUM AND MANGANESE PRECURSORS TO FORM POLYCRYSTALLINE 10 μm, HOLLOW $LiMn_2O_4$ PARTICLES, SAADATKHAH ET AL.[79]

Our sample of 6225 articles from the WoS has four times as many articles mentioning spray pyrolysis (47) versus melt synthesis/casting (12).[22,41,80–82] A study on ultrasonic spray pyrolysis of C-LFP was cited over 200 times as of late 2017.[83] However, fewer than six research groups work with flame-assisted spray pyrolysis.[28,29,84–86] This emerging technique controls purity and carbon from the flame coats the particle surface, which helps reduce manufacturing costs. In this study, rather than Fe, $Mn(NO_3)_2$ reacts with $LiNO_3$ to form $LiMn_2O_4$. The main factors controlling Mn_3O_4 content and purity are temperature and droplet size, while fuel and precursor type affect carbon content: it reaches 2 % with carbonate and acetate precursors but is as low as 0.1 % with nitrate precursors.

Spray pyrolysis belongs to the red cluster in the bibliographic map and is at the far outer left edge. Its greatest link is with C-LFP. Among the articles citing manufacturing methods, the most frequent is hydrothermal synthesis (323 occurrences), followed by coprecipitation (117), solvothermal (117), solid state reaction (110), and carbothermal reduction (103).

CONCLUSIONS

Cost and performance of lithium-ion batteries has improved over the last twenty years: energy density has tripled to 700 $W \cdot h \cdot L^{-1}$ and cost has dropped from 4500 to 150 $/kWh.[87] As the market continues to grow, the price of batteries based on Co and Ni might also increase, which motivates some manufactures to skimp on environmental stewardship and safety.[88]

The benefits of liquid metal synthesis to produce LFP include: utilization of low grade, inexpensive precursors, a homogeneous liquid composition, scale-up readiness, and similar or even better performance. If successful at the commercial scale, this process represents a paradigm shift for positive electrode materials that will result in much lower costs and open up new markets and opportunities beyond automotives.

ACKNOWLEDGEMENTS

The authors gratefully acknowledge the financial support of Johnson-Matthey Battery Materials (grant 05 0589 05), Natural Sciences and Engineering Research Council of Canada (grant APCPJ-435543-2012), and the Canada Foundation for Innovation grant (FCI 30634) obtained through the Automotive Partnership Canada program.

NOMENCLATURE

CLFP	carbon coated lithium iron phosphate
CNT	carbon nanotubes
DFT	density functional theory
EV	electric vehicle
HEV	hybrid electric vehicle
LFP	$LiFePO_4$—lithium iron phosphate
N_{IF}	journal impact factors indexed by JCR in 2015
N_{art}	total number of articles per subject reference
N_j	number of journals per WoS category
N_p	total number of patents per Derwent subject
NP	nanoparticles
NT	nanotube
SEM	scanning electron microscopy
SOC	state of charge
T	temperature
TEM	transmission electron microscopy
XANES	x-ray absorption near edge structure
XAS	x-ray adsorption spectroscopy
XPS	x-ray photoelectron spectroscopy
XRD	x-ray diffraction

REFERENCES

[1] A. Padhi, K. Nanjundaswamy, J. Goodenough, *J. Electrochem. Soc.* **1997**, *144*, 1188.

[2] A. Padhi, K. Nanjundaswamy, C. Masquelier, S. Okada, J. Goodenough, *J. Electrochem. Soc.* **1997**, *144*, 1609.

[3] Clarivate Analytics, *Web of Science Core Collection*^{TM}, **2017**, accessed on 7 August 2017, http://apps.webofknowledge.com.

[4] Clarivate Analytics, *Derwent Innovations Index*, **2017**, accessed on 9 September 2017, http://apps.webofknowledge.com.

[5] CN104577093-A (**2015**), Y. Mao, T. Han.

[6] CN104409730-A (**2015**), S. Qiu, Z. Zhang, D. Li, Y. Liu, R. Meng, J. Peng.

[7] US 2010/0015514 A1 (**2010**), H. Miyagi, R. Kato, M. Yokomizo, H. Uono, H. Matsumoto, T. Santou, M. Kotato, T. Nakajima, H. Suzuki, H. Oshima.

[8] A. Yamada, S. Chung, K. Hinokuma, *J. Electrochem. Soc.* **2001**, *148*, A224.

[9] J. B. Leriche, S. Hamelet, J. Shu, M. Morcrette, C. Masquelier, G. Ouvrard, M. Zerrouki, P. Soudan, S. Belin, E. Elkaim, F. Baudelet, *J. Electrochem. Soc.* **2010**, *157*, A606.

[10] M. Sun, H. Liu, J. Qu, J. Li, *Adv. Energy Mater.* **2016**, *6*, 1600087.

[11] B. Kang, G. Ceder, *Nature* **2009**, *458*, 190.

[12] B. Scrosati, J. Garche, *J. Power Sources* **2010**, *195*, 2419.

[13] B. L. Ellis, W. R. M. Makahnouk, Y. Makimura, K. Toghill, L. F. Nazar, *Nat. Mater.* **2007**, *6*, 749.

[14] S. Yang, P. Zavalij, M. Whittingham, *Electrochem. Commun.* **2001**, *3*, 505.

[15] I. D. Johnson, M. Luebke, O. Y. Wu, N. M. Makwana, G. J. Smales, H. U.Islam, R. Y. Dedigama, R. I. Gruar, C. J. Tighe, D. O. Scanlon, F. Cora, D. J. L. Brett, P. R. Shearing, J. A. Darr, *J. Power Sources* **2016**, *302*, 410.

[16] J. R. Nair, M. Destro, F. Bella, G. B. Appetecchi, C. Gerbaldi, *J. Power Sources* **2016**, *306*, 258.

[17] L. Dimesso, C. Foerster, W. Jaegermann, J. P. Khanderi, H. Tempel, A. Popp, J. Engstler, J. J. Schneider, A. Sarapulova, D. Mikhailova, L. A. Schmitt, S. Oswald, H. Ehrenberg, *Chem. Soc. Rev.* **2012**, *41*, 5068.

[18] W. Ren, K. Wang, J. Yang, R. Tan, J. Hu, H. Guo, Y. Duan, J. Zheng, Y. Lin, F. Pan, *J. Power Sources* **2016**, *331*, 232.

[19] K. Dokko, S. Koizumi, H. Nakano, K. Kanamura, *J. Mater. Chem.* **2007**, *17*, 4803.

[20] K. Saravanan, P. Balaya, M. V. Reddy, B. V. R. Chowdari, J. J. Vittal, *Energ. Environ. Sci.* **2010**, *3*, 457.

[21] K. M. O. Jensen, C. Tyrsted, M. Bremholm, B. B. Iversen, *ChemSusChem* **2014**, *7*, 1594.

[22] S. E. Khakani, D. Rochefort, D. D. MacNeil, *J. Electrochem. Soc.* **2016**, *163*, A1311.

[23] S. Franger, F. L. Cras, C. Bourbon, H. Rouault, *J. Power Sources* **2003**, *119*, 252.

[24] D. Choi, P. N. Kumta, *J. Power Sources* **2007**, *163*, 1064.

[25] S. W. Oh, S.-T. Myung, S.-M. Oh, K. H. Oh, K. Amine, B. Scrosati, Y.-K. Sun, *Adv. Mater.* **2010**, *22*, 4842.

[26] S. Bewlay, K. Konstantinov, G. Wang, S. Dou, H. Liu, *Mater. Lett.* **2004**, *58*, 1788.

[27] M. Konarova, I. Taniguchi, *J. Power Sources* **2010**, *195*, 3661.

[28] P. M. Pratheeksha, E. H. Mohan, B. V. Sarada, M. Ramakrishna, K. Hembram, P. V. V. Srinivas, P. J. Daniel, T. N. Rao, S. Anandan, *Phys. Chem. Chem. Phys.* **2017**, *19*, 175.

[29] F. Krumeich, O. Waser, S. E. Pratsinis, *J. Solid State Chem.* **2016**, *242*, 96.

[30] J. Yang, J. Xu, *J. Electrochem. Soc.* **2006**, *153*, A716.

[31] T. Muraliganth, K. R. Stroukoff, A. Manthiram, *Chem. Mater.* **2010**, *22*, 5754.

[32] A. V. Murugan, T. Muraliganth, A. Manthiram, *J. Phys. Chem. C* **2008**, *112*, 14665.

[33] J. V. Laveda, V. Chandhok, C. A. Murray, G. W. Paterson, S. A. Corr, *Chem. Commun.* **2016**, *52*, 9028.

[34] K. J. Kreder, A. Manthiram, *ACS Energy Letters* **2017**, *2*, 64.

[35] G. Tan, F. Wu, L. Li, R. Chen, S. Chen, *J. Phys. Chem. C* **2013**, *117*, 6013.

[36] N. J. vanEck, L. Waltman, *Science* **2010**, *84*, 523.

[37] W. Kasprzak, D. Li, G. S. Patience, P. Sauriol, H. Villazon-Amars, M. Dolle, M. Gauthier, S. Rousselot, M. Talebi-Esfandarani, T. Bibienne, X. Sun, Y. Liu, G. Liang, *Journal of Advanced Materials and Processing* **2017**, *175*, 16.

[38] D. Li, W. Kasprzak, G. S. Patience, P. Sauriol, H. Villazon-Amars, M. Dolle, M. Gauthier, S. Rousselot, M. Talebi-Esfandarani, T. Bibienne, X. Sun, Y. Liu, G. Liang, "Production of Lithium-Ion Cathode Material for Automotive Batteries Using Melting Casting Process," *9th International Symposium on High-Temperature Metallurgical Processing*, Springer International Publishing, Berlin **2018**.

[39] CA2510880-A1 (**2007**), M. Gauthier.

[40] CA2566906-A1 (**2008**), N. Ravet, M. Gauthier, T. Lahrs, G. Liang, C. Michot, R. Nathalie, G. Michel, L. Thorsten, M. Christophe.

[41] M. Gauthier, C. Michot, N. Ravet, M. Duchesneau, J. Dufour, G. Liang, J. Wontcheu, L. Gauthier, D. D. MacNeil, *J. Electrochem. Soc.* **2010**, *157*, A453.

[42] D. D. MacNeil, L. Devigne, C. Michot, I. Rodrigues, G. Liang, M. Gauthier, *J. Electrochem. Soc.* **2010**, *157*, A463.

[43] P. Sauriol, D. Li, L. Hadidi, H. Villazon-Amars, L. Jin, B. Yari, M. Gauthier, M. Dolle, P. Chartrand, W. Kasprzak, G. Liang, G. S. Patience, *Can. J. Chem. Eng.* **2019**, *97*, 2196.

[44] M. N. Banis, Z. Wang, S. Rousselot, Y. Liu, Y. Hu, M. Talebi-Esfandarani, T. Bibienne, M. Gauthier, R. Li, G. Liang, M. Dolle, P. Sauriol, T.-K. Sham, X. Sun, *Can. J. Chem. Eng.* **2019**, *97*, 2211.

[45] M. Talebi-Esfandarani, S. Rousselot, M. Gauthier, P. Sauriol, G. Liang, M. Dolle, *J. Solid State Electrochem.* **2016**, *20*, 1821.

[46] M. Talebi-Esfandarani, S. Rousselot, M. Gauthier, P. Sauriol, M. Duttine, A. Wattiaux, Y. Liu, A. X. Sun, G. Liang, M. Dolle, *J. Solid State Electrochem.* **2016**, *20*, 3481.

[47] C. Ban, W.-J. Yin, H. Tang, S.-H. Wei, Y. Yan, A. C. Dillon, *Adv. Energy Mater.* **2012**, *2*, 1028.

[48] H. Liu, Q. Cao, L. J. Fu, C. Li, Y. P. Wu, H. Q. Wu, *Electrochem. Commun.* **2006**, *8*, 1553.

[49] M. Talebi-Esfandarani, O. Savadogo, *Solid State Ionics* **2014**, *261*, 81.

[50] M. Talebi-Esfandarani, O. Savadogo, *J. Appl. Electrochem.* **2014**, *44*, 555.

[51] D. Wang, H. Li, S. Shi, X. Huang, L. Chen, *Electrochim. Acta* **2005**, *50*, 2955.

[52] C. S. Sun, Z. Zhou, Z. G. Xu, D. G. Wang, J. P. Wei, X. K. Bian, J. Yan, *J. Power Sources* **2009**, *193*, 841.

[53] Y. Hu, M. Doeff, R. Kostecki, R. Finones, *J. Electrochem. Soc.* **2004**, *151*, A1279.

[54] Y. Liu, M. N. Banis, W. Xiao, R. Li, Z. Wang, K. R. Adair, S. Rousselot, P. Sauriol, M. Dolle, G. Liang, T.-K. Sham, X. Sun, *Can. J. Chem. Eng.* **2019**, *97*, 2218.

[55] A. T. Phan, A. Gheribi, P. Chartrand, *Can. J. Chem. Eng.* **2019**, *97*, 2224.

[56] S. Furutsuki, S.-C. Chung, S. ichi Nishimura, Y. Kudo, K. Yamashita, A. Yamada, *J. Phys. Chem. C* **2012**, *116*, 15259.

[57] L. Jin, J. Wang, S. Rousselot, M. Dollé, P. Chartrand, *Can. J. Chem. Eng.* **2019**, *97*, 2234.

[58] A. T. Dinsdale, *Calphad* **1991**, *15*, 317.

[59] H. Li, M. Rostamizadeh, K. Mameri, D. C. Boffito, N. Saadatkhah, M. G. Rigamonti, G. S. Patience, *Can. J. Chem. Eng.* **2019**, *97*, 2242.

[60] H. Li, A. Ndjamo, P. Sauriol, G. S. Patience, *Adv. Powder Technol.* **2017**, *28*, 1000.

[61] T. Drezen, N.-H. Kwon, P. Bowen, I. Teerlinck, M. Isono, I. Exnar, *J. Power Sources* **2007**, *174*, 949.

[62] M. Rigamonti, Y.-X. Song, H. Li, N. Saadatkhah, P. Sauriol, G. S. Patience, *Can. J. Chem. Eng.* **2019**, *97*, 2251.

[63] F. Yu, J.-J. Zhang, Y.-F. Yang, G.-Z. Song, *J. Mater. Chem.* **2009**, *19*, 9121.

[64] Y.-J. Lv, Y.-F. Long, J. Su, X.-Y. Lv, Y.-X. Wen, *Electrochim. Acta* **2014**, *119*, 155.

[65] J. Ren, W. Pu, X. He, C. Jiang, C. Wan, *Ionics* **2011**, *17*, 581.

[66] X. Yang, S. M. Zhang, J. X. Zhang, M. Y. Xu, P. Ren, X. C. Li, L. C. Yan, *Funct. Mater. Lett.* **2011**, *4*, 323.

[67] R. Mei, Y. Yang, X. Song, Z. An, J. Zhang, *Electrochim. Acta* **2015**, *153*, 523.

[68] J.-F. Zhang, C. Shen, B. Zhang, J. C. Zheng, C. L. Peng, X. W. Wang, X. B. Yuan, H. Li, G. M. Chen, *J. Power Sources* **2014**, *267*, 227.

[69] M. Brisbois, S. Caes, M. T. Sougrati, B. Vertruyen, A. Schrijnemakers, R. Cloots, N. Eshraghi, R. P. Hermann, A. Mahmoud, F. Boschini, *Sol. Energ. Mat. Sol. C.* **2016**, *148*, 67.

[70] B. Zou, Y. Wang, S. Zhou, *Mater. Lett.* **2013**, *92*, 300.

[71] N. Saadatkhah, M. G. Rigamonti, D. C. Boffito, H. Li, G. S. Patience, *Powder Technol.* **2017**, *316*, 434.

[72] S. Aghaee-Sarbarze, M. Latifi, M. Rasouli, P. Sauriol, J. Chaouki, *Can. J. Chem. Eng.* **2019**, *97*, 2259.

[73] D. Geldart, *Powder Technol.* **2018**, *7*, 285.

[74] I. Taniguchi, R. Tussupbayev, *Chem. Eng. J.* **2012**, *192*, 334.

[75] J. Wang, F. Cai, G. Yang, B. Wang, S. Hu, *Rare Metal Mat. Eng.* **2015**, *44*, 307.

[76] B. Yari, P. Sauriol, J. Chaouki, *Can. J. Chem. Eng.* **2019**, *97*, 2273.

[77] S. Vyazovkin, D. Dollimore, *J. Chem. Inf. Comp. Sci.* **1996**, *36*, 42.

[78] H. Villazon, P. Sauriol, M. Talebi-Esfandarani, S. Rousselot, T. Bibienne, M. Dollé, P. Chartrand, M. Gauthier, G. Liang, *Can. J. Chem. Eng.* **2019**, *97*, 2287.

[79] N. Saadatkhah, S. F. Aghamiri, M. R. Talaie, G. Patience, *Can. J. Chem. Eng.* **2019**, *97*, 2299.

[80] K. Zaghib, P. Charest, M. Dontigny, A. Guerfi, M. Lagace, A. Mauger, M. Kopec, C. M. Julien, *J. Power Sources* **2010**, *195*, 8280.

[81] T. Togashi, T. Honma, T. Komatsu, *J. Ceram. Soc. Jpn.* **2015**, *123*, 26.

[82] T. Nagakane, H. Yamauchi, K. Yuki, M. Ohji, A. Sakamoto, T. Komatsu, T. Honma, M. Zou, G. Park, T. Sakai, *Solid State Ionics* **2012**, *206*, 78.

[83] S.-M. Oh, S.-W. Oh, C.-S. Yoon, B. Scrosati, K. Amine, Y.-K. Sun, *Adv. Funct. Mater.* **2010**, *20*, 3260.

[84] N. A. Hamid, S. Wennig, A. Heinzel, C. Schulz, H. Wiggers, *Ionics* **2015**, *21*, 1857.

[85] O. Waser, O. Brenner, A. J. Groehn, S. E. Pratsinis, *Chem. Process. Eng.-Inz.* **2017**, *38*, 51.

[86] A. Halim, W. Widiyastuti, H. Setyawan, S. Machmudah, T. Nurtono, S. Winardi, *5th Nanoscience and Nanotechnology Symposium (NNS2013)* **2014**, *1586*, 173.

[87] K. Turcheniuk, D. Bondarev, V. Singhal, G. Yushin, *Nature* **2018**, *559*, 467.

[88] P. Whoriskey, T. C. Frankel, Y. Wang, X. Jing, *Washington Post* 2 October 2016.

Manuscript received September 7, 2018; accepted for publication September 10, 2018.